Arch Toxicol (2010) 84:183–190
DOI 10.1007/s00204-009-0488-x

TOXICOKINETICS AND METABOLISM

Biodistribution and toxicity of intravenously administered silica nanoparticles in mice

Guangping Xie · Jiao Sun · Gaoren Zhong · Liyi Shi · Dawei Zhang

Received: 17 August 2009 / Accepted: 28 October 2009 / Published online: 20 November 2009
© Springer-Verlag 2009

Abstract As the biosafety of nanotechnology becomes a growing concern, the in vivo nanotoxicity of NPs has drawn a lot of attention. Silica nanoparticles (SiNPs) have been widely developed for biomedical use, but their biodistribution and toxicology have not been investigated extensively in vivo. Although investigations of in vivo qualitative distribution of SiNPs have been reported, the time-dependent and quantitative informations about the distribution of SiNPs are still lacking. Here we investigated the long-term (30 days) quantitative tissue distribution, and subcellular distribution, as well as potential toxicity of two sizes of intravenously administered SiNPs in mice using radiolabeling, radioactive counting, transmission electron microscopy and histological analysis. The results indicated that SiNPs accumulate mainly in lungs, liver and spleen and are retained for over 30 days in the tissues because of the endocytosis by macrophages, and could potentially cause liver injury when intravenously injected.

Keywords Tissue distribution · Nanotoxicity · Silica nanoparticles · Quantitative · Endocytosis

G. Xie · J. Sun (✉)
Shanghai Biomaterials Research & Testing Center,
Shanghai Ninth People's Hospital,
Shanghai Jiaotong University School of Medicine,
Shanghai, China
e-mail: jiaosun59@yahoo.com

G. Zhong
School of Pharmacy, Fudan University, Shanghai, China

L. Shi · D. Zhang
Nano-Science & Technology Research Center,
Shanghai University, Shanghai, China

Introduction

Silica nanoparticles (SiNPs) possess extraordinary properties, such as monodispersity, large surface area, high drug loading efficiency, and potential for hybridization with other organic/inorganic materials (Iezzi et al. 2002; Yang et al. 2008). These extraordinary properties allowe SiNPs to be widely developed for biomedical use, including optical imaging (Zhao et al. 2004), cancer therapy (Hirsch et al. 2003), targeted drug delivery (Huo et al. 2006) and controlled drug release for genes and proteins (Roy et al. 2005; Slowing et al. 2007).

However, the versatile biomedical use of SiNPs could cause new side effects. As the biosafety of nanotechnology becomes a growing concern, attention has been paid on the toxicity of nanoparticles (NPs)(Maynard et al. 2006; Tsuji et al. 2006). Although NPs could induce cell damage and apoptosis in vitro (Wang et al. 2007), currently, it is unclear whether NPs exposure produces harmful biological responses in vivo (Stern and McNeil 2008). Hence, the nanotoxicology as a new subdiscipline of nanotechnology is growing need to in vivo study (Fischer and Chan 2007; Oberdorster et al. 2005). To evaluate the in vivo nanotoxicity, it is essential to understand some pharmacological information of in vivo NPs. Due to the lack of suitable tracking methods, pharmacokinetics of SiNPs has not been reported extensively, in contrast to the significant number of studies on the orther NPs such as iron oxide magnetic nanoparticles, titanium dioxide nanoparticles, and gold nanoparticles (Fabian et al. 2008; Jain et al. 2008; Sonavane et al. 2008). Recently, some investigations were focusing on the in vivo distributon of SiNPs and some documents were reported. Choi and colleagues (Choi et al. 2007) showed that core–shell silica nanoparticles containing quantum dots localized predominantly in the spleen and

liver, and were cleared from the liver over approximately 60 days. He and colleagues (He et al. 2008) synthesized different surface-modified silica nanoparticles and investigated their biodistribution and urinary excretion both in vivo and ex vivo. However, these studies were qualitative and do not provide quantitative information about SiNPs in vivo. Moreover, although the tissues in which most SiNPs are located in vivo are clear, time-dependent and quantitative informations about the distribution of SiNPs in these tissues are lacking. We need to understand how long and what quantity of SiNPs are retained, as well as why SiNPs accumulate in these tissues. These issues closely correlate with the in vivo nanotoxicity of SiNPs. Otherwise, when SiNPs are designed as drug delivery carriers, the pharmacokinetic profiles of the parent drug and the drug encapsulated in the nanoparticles are often different. Therefore, monitoring the quantitative biodistribution of SiNPs, and analyzing the localization mechanism, will improve our understanding their efficacy and side effects for the pharmacological use.

Herein, we investigated the biodistribution of intravenously administered SiNPs, including long-term quantitative tissue distribution, and subcellular distribution. In order to analyze the toxicity of SiNPs, the pathological changes in the tissues in which the SiNPs were primarily localized were investigated to evaluate the potential toxicity of SiNPs. The SiNPs we used were modified with aminopropyltriethoxysilane (APTS) to introduce amino groups on the surface. We labeled the modified SiNPs with radioactive iodine (^{125}I) and used a γ-counter to assess quantitatively the tissue distribution in mice. Two sizes of SiNPs were investigated, providing a more complete understanding of the in vivo behaviors of SiNPs.

Materials and methods

Synthesis, modification and characterization of SiNPs

Two sizes of SiNPs were synthesized by varying the ratios of tetraethylorthosilicate (TEOS), ammonium hydroxide, and deionized water, according to previously published procedures (Lipski et al. 2008). Briefly, two solutions were prepared: one containing TEOS and ethanol (EtOH), and the other composed of ammonium hydroxide, deionized water and EtOH. The ammonium–water–EtOH solution was slowly added to the TEOS–EtOH solution, with stirring, and the final mixture was stirred overnight to allow the SiNPs to coarsen. After two alcohol washes, SiNPs were obtained by vacuum drying. The resulting SiNPs were modified as necessary by a previously published method (Pham et al. 2007). Briefly, APTS in EtOH [2% (v%)] was adjusted to pH 3.5 using oxalic acid and stirred for 1 h at room temperature. Thereafter, SiNPs were added at a concentration of 10% and incubated with stirring for 6 h at 60°C. After vacuum drying, washing with alcohol and vacuum drying again, the modified SiNPs were collected.

After modification, the physical and chemical properties of SiNPs were characterized. The SiNPs structures were confirmed by TEM (JEM-2010, JEOL Ltd, Japan). The size distribution was analyzed by laser scattering (ELS-Z, Otsuka Electronics, Japan). Fourier transform infrared (FTIR) spectral (EQUINOX 55, Bruker Co, Germany) analysis was used to confirm the characteristic bands of the modified SiNPs.

Radiolabeling of SiNPs with ^{125}I

A test tube was coated with 25 μl Bolton-Hunter reagent (10 mg/ml in benzene) and subsequently was dried with a gentle stream of nitrogen for 30–60 min. Dimethylformamide (DMF; 2 μl) and Na^{125}I (60 MBq; 1.5 μl) were incubated at room temperature with 1.5 μl chloramine (4 mg/ml) in the coated test tube. The modified SiNPs [100 mg in 50 μl 0.05 M borate buffer (pH 8.4)] were added, stirred, and incubated on ice for 30 min. The reaction was terminated by addition of 200 μl borate buffer supplemented with 0.2 M glycine. After the separation of ^{125}I-labeled SiNPs (^{125}I-SiNPs) by column chromatography, 2 μl of the resulting solution was extracted and subjected to paper chromatography using instant thin layer chromatography–silica gel (ITLC-SG), with 2.5% bovine serum albumin (w/w) in 0.01 M phosphate buffered saline (pH 7.4) as the solvent, and a γ-counter (Shanghai Institute of Nuclear Instrument Factory, China) to identify the radioactive substance. Before the in vivo assay, the stability of ^{125}I-SiNPs was analyzed in vitro. The ^{125}I-SiNPs were dissolved in physiological saline containing 10% (v%) mouse serum and incubated at 37°C. At five time points (1, 3, 7, 15, and 30 days), 2 μl of ^{125}I-SiNPs suspension were extracted and analyzed by paper chromatography using ITLC-SG as described above. The stablity of ^{125}I-SiNPs was expressed as the percentage of radioactivity at the site of ^{125}I- SiNPs compared with the total radioactivity on the paper. After vacuum drying, both ^{125}I-SiNPs were collected. The specific activity of SiNPs20 and SiNPs80 were 5.06×10^5 Bq/mg and 4.73×10^5 Bq/mg, respectively.

Animals and treatment

For the in vivo studies, 7-week-old male ICR mice, weighing 20 ± 1 g, were purchased from SLACCAS Laboratory Animal Co, Ltd (Shanghai, China) and injected intravenously via the tail vein with ^{125}I-SiNPs for the evaluation of long-term quantitative tissue distribution, or modified SiNPs for the evaluation of subcellular distribution as well as

pathological assays. The concentration and injected dose of SiNPs were 1 mg/ml in physiological saline and10 mg/kg body weight, respectively. Animals were group-housed in stainless steel cages under standard environmental conditions (25 ± 1°C, 55 ± 5% humidity and a 12/12 h light/dark cycle) and maintained with free access to water and a standard laboratory diet (35% carbohydrate, 25% protein, 15% lipids, 3% vitamins). The animal experiment was approved by the Animal Ethical Committee of Shanghai Jiaotong University (China).

Evaluation of tissue distribution

The long-term quantitative tissue distribution was evaluated over 30 days at 5 time points (1, 3, 7, 15, and 30 days) after injected with both ^{125}I-SiNPs. Five animals per group were sacrificed at each time point. Blood and tissues, including heart, lungs, liver, spleen, kidneys, stomach, intestine, brain and bone, were harvested, weighed, and counted for 1 min in a γ-counter to detect the tissue radioactivity. The tissue distribution was expressed as the percentage injected dose per gram tissue (% ID/g).

Evaluation of subcellular distribution

Both sizes of SiNPs modified with APTS and physiological saline as a control, were injected intravenously. After 7 days, animals ($n = 3$) were sacrificed and liver and spleen were removed and immersion-fixed in glutaral for 24 h at room temperature. Tissue sections (40 nm) were prepared after dehydration and embedded in epoxy resin. The sections were stained with lead citrate and subsequently processed for subcellular evaluation of SiNPs distribution by TEM.

Toxicologic assay

According to the Organization for economic cooperation and development (OECD) guidelines for the testing of chemicals (method No. 417), both modified SiNPs and physiological saline as a control were injected once a day. After sequential injection for 7 days, animals ($n = 3$) were sacrificed and lungs, liver, spleen were excised and fixed in 10% buffered formalin-saline at 4°C overnight and then embedded in paraffin blocks. Tissue sections of 4 μm thickness were prepared and stained with hematoxylin and eosin (H&E). The tissue morphology was observed under a microscope at 400× magnification.

Statistical analysis

The radioactivity of the materials was determined from following equation: $C = C_0 \times e^{-(0.693159t/T)}$, where C was the actual radioactivity, C_0 was the measured radioactivity, T was the half-life of ^{125}I (59.6 days), and t was the time interval between C and C_0. Compiled data were presented as mean ± standard deviation. Where feasible, the data were analyzed for statistical significance by the student's t-test. For all tests, significance was set at the 95% confidence level.

Results

Physicochemical properties of SiNPs

The size distributions of both SiNPs were about 20 nm (SiNPs20) and 80 nm (SiNPs80), respectively (Fig. 1). TEM images, obtained after dispersion of the sample onto a TEM grid and evaporation of the solvent, indicated SiNP were granular (Fig. 2).

Identification and stablity of ^{125}I-SiNPs

The identification and stability of radioactive materials after the radiolabelling were analyzed in vitro by paper chromatography and the results were showed in Fig. 3. It can be observed that the ^{125}I moved toward the solvent front (Rf = 0.9) faster than ^{125}I-BH (Rf = 0.7), but the ^{125}I-SiNPs remained at the point of spotting (Rf = 0). The ^{125}I-SiNPs were stable for 30 days in vitro, and the purity of the ^{125}I-SiNPs was consistently greater than 95%.

Long-term quantitative tissue distribution

The long-term quantitative tissue distribution was evaluated over 30 days at five time points (1, 3, 7, 15, and 30 days) after injection and its result was expressed as % ID/g in Table 1. The distribution patterns of the two

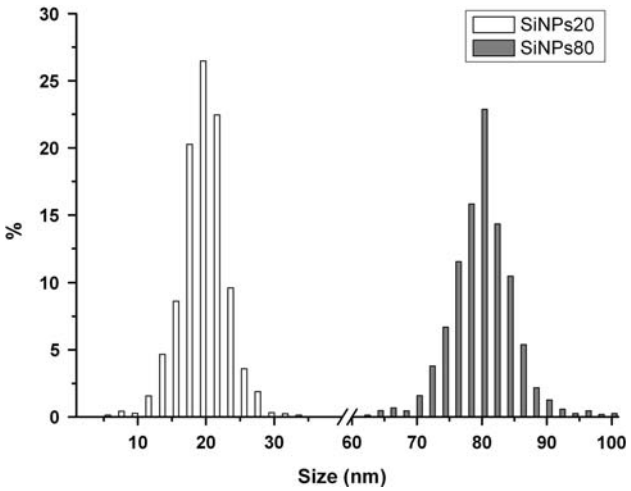

Fig. 1 Size distribution of SiNPs determined by laser scattering

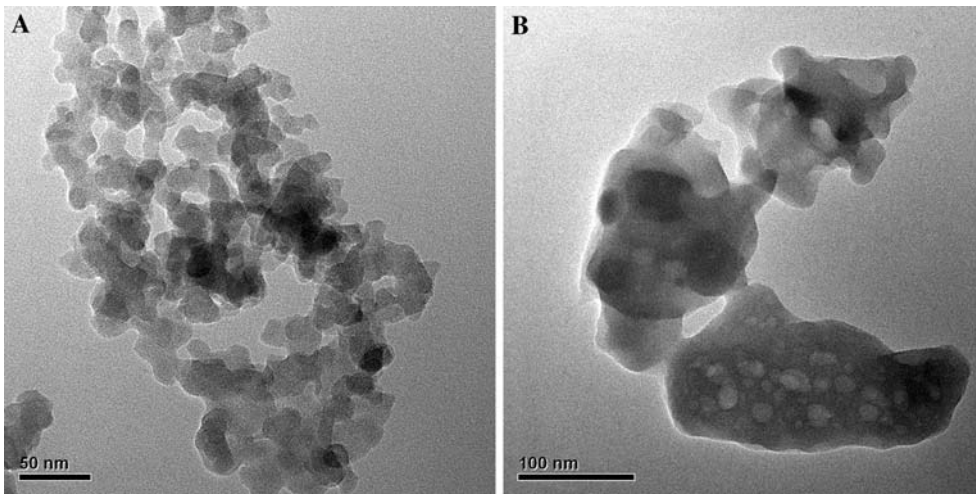

Fig. 2 TEM images of SiNPs20 (**a**) and SiNPs80 (**b**)

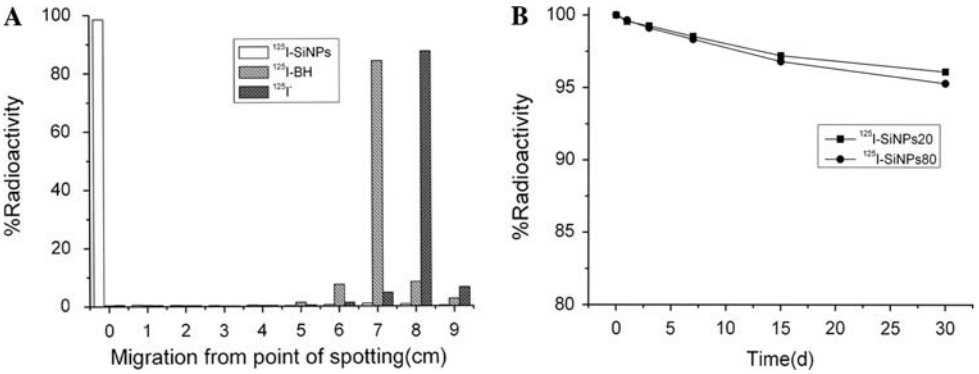

Fig. 3 The identification (**a**) and stability (**b**) of ^{125}I-SiNPs. After radiolabelling with ^{125}I, the identification and stability of ^{125}I-SiNPs were analized by paper chromatography using ITLC-SG with 2.5% BSA (w/w) in 0.01 M PBS (pH 7.4) as the solvent. The results were expressed as the percentage of radioactivity at the site of ^{125}I-SiNPs compared with the total radioactivity on the paper

different sizes of SiNPs were similar. After intravenous injection, both sizes of SiNPs accumulated primarily in liver, spleen and lungs, but rarely in the blood, heart, kidneys, intestine, stomach and brain. The amount of SiNPs20 in these tissues was higher than that of SiNPs80. Figure 4 shows that the changes in tissue distribution, after intravenous injection of both sizes of SiNPs, were time-dependent. Accumulation of both SiNPs peaked at 1 day, the first time point after injection, and then gradually declined over the next four time points. The changes in SiNPs distribution varied between these tissues. The accumulation of SiNPs80 in lungs was reduced from 27% at 1 day to 2% at 7 days, and reduced moderately at 15 and 30 days, while accumulation of SiNPs20 was reduced briefly from 15% at 1 day to 6% at 3 days, and reduced moderately at 15 and 30 days. Figure 4 also shows the distribution changes of both SiNPs in the liver and spleen, SiNPs20 levels decreased visibly over time, but SiNPs80 decreased only slightly.

Subcellular distribution of SiNPs

Figure 5 shows the subcellular distribution of SiNPs in main accumulated tissues. SiNPs were taken up mainly by macrophages in liver and spleen, and rarely appeared in other cells of these tissues. The figure also indicates that endocytosis and engulfment by phagosomes may be the primary way that SiNPs get into the cells.

Toxicity of SiNPs

The results of toxicologic assay, expressed in Fig. 6, show lungs and spleen did not display significant changes in morphology, but apparent pathological changes, including a mononuclear inflammatory infiltrate at the portal area and hepatocyte necrosis at the portal triads, were observed in liver.

Discussion

As known, it is very difficult to track and detect the SiNPs in vivo. Although there are some literatures about the qualitative in vivo distribution of SiNPs, quantitative distribution findings are lacking. The present study is the first quantitative investigation about in vivo distribution of SiNPs. The results were carried out by radioactive iodine labeling and radioactive counting. In order to accomplish

Table 1 Tissue distribution of two sizes of SiNPs

	1 day		3 days		7 days		15 days		30 days	
	SiNPs20	SiNPs80	SiNPs20	SiNPs80	SiNPs20	SiNPs80	SiNPs20	SiNPs80	SiNPs20	SiNPs80
Blood	0.06 ± 0.02	0.06 ± 0.01	0.02 ± 0.01	0.03 ± 0.01	0.02 ± 0.00	0.02 ± 0.00	0.01 ± 0.00	0.01 ± 0.00	0.01 ± 0.00	0.01 ± 0.00
Heart	0.51 ± 0.10	0.69 ± 0.23	0.32 ± 0.22	0.14 ± 0.03	0.29 ± 0.07	0.04 ± 0.01	0.30 ± 0.11	0.04 ± 0.01	0.20 ± 0.09	0.02 ± 0.01
Lungs	14.96 ± 4.41	26.9 ± 2.83	6.25 ± 3.13	6.94 ± 1.74	5.33 ± 1.75	1.74 ± 1.05	3.73 ± 1.50	0.93 ± 0.23	1.95 ± 1.44	0.31 ± 0.11
Liver	43.29 ± 5.79*	13.64 ± 1.38	36.98 ± 8.62*	13.21 ± 1.91	30.31 ± 6.33*	12.98 ± 1.02	22.06 ± 4.22*	8.89 ± 0.66	16.80 ± 1.96*	5.79 ± 0.68
Spleen	48.73 ± 8.49*	5.89 ± 1.63	41.11 ± 7.29*	4.01 ± 0.45	27.32 ± 7.70*	3.63 ± 0.92	17.80 ± 4.40*	3.39 ± 0.93	15.01 ± 1.46*	2.21 ± 0.22
Kidney	0.62 ± 0.21	0.3 ± 0.08	0.28 ± 0.11	0.13 ± 0.04	0.24 ± 0.04	0.04 ± 0.01	0.19 ± 0.05	0.03 ± 0.01	0.11 ± 0.04	0.03 ± 0.02
Intestine	0.16 ± 0.03	0.08 ± 0.02	0.06 ± 0.02	0.06 ± 0.03	0.04 ± 0.01	0.02 ± 0.01	0.03 ± 0.00	0.01 ± 0.00	0.03 ± 0.01	0.01 ± 0.00
Stomach	0.19 ± 0.03	0.18 ± 0.06	0.09 ± 0.02	0.16 ± 0.08	0.14 ± 0.12	0.04 ± 0.01	0.07 ± 0.06	0.06 ± 0.07	0.09 ± 0.04	0.01 ± 0.00
Brain	0.02 ± 0.01	0.1 ± 0.08	0.01 ± 0.01	0.02 ± 0.01	0.00 ± 0.00	0.01 ± 0.00	0.00 ± 0.00	0.01 ± 0.00	0.00 ± 0.00	0.00 ± 0.00
Bone	2.38 ± 0.78	0.29 ± 0.09	1.46 ± 0.44	0.21 ± 0.08	1.75 ± 0.69	0.13 ± 0.06	1.49 ± 0.44	0.22 ± 0.08	0.83 ± 0.18	0.15 ± 0.05

Animals were injected with ^{125}I-SiNPs and sacrificed at 1, 3, 7, 15 and 30 days after injection. Tissues were harvested, weighed, and counted for 1 min in a γ-counter to detect the tissue radioactivity. The tissue distribution was expressed as % ID/g and the data were showed as the mean ± SD of five independent experiments in the table

* $P < 0.05$ vs. SiNPs80

the radiolabelling, the SiNPs we used were modified with APTS to introduce amino groups onto the surface. Numerous methods have been developed for surface modification of SiNPs in order to enable the coupling of SiNPs to biomolecular targets (Mader et al. 2008). Different functional groups, including amino groups, can be introduced easily onto the SiNPs for conjugation with biomolecules. The silica surface modification makes such NPs chemically inert and physically stable. These properties make SiNPs excellent labeling reagents for bioanalysis and bioimaging techniques (Bagwe et al. 2006). In addition, unmodified SiNPs acting as drug carriers rapidly release the drug (Li et al. 2004). To induce sustained release, SiNPs require surface modification (Kim et al. 2006).

We demonstrated that the tissues in which SiNPs mainly accumulated were liver, spleen and lungs. Although the endothelial wall is the primary barrier to nanoparticle delivery, the leaky structure of the endothelial wall in certain tissues, such as tumors, liver, spleen or bone marrow, allows nanoparticles to be taken up. Unlike small molecule drugs that can diffuse through the capillary wall into the tissue, nanoparticles pass through the gaps between the cells of endothelium (Li and Huang 2008). Therefore, the size of NPs will impact their in vivo permeability and thus their uptake by the certain tissues. Small NPs pass more easily through the gaps and accumulate in certain tissues than large NPs (Torchilin et al. 2003). Our results that the amount of SiNPs20 in liver and spleen were higher than that of SiNPs80 meet this inference. However, we also found that significant amounts of both sizes of SiNPs distributed in lungs at 1 day after injection, even though lungs do not have a leaky endothelial wall, and deceased visibly within 7 days. This accumulation in lungs maybe due to the aggregation of SiNPs. The aggregates are large and often cause transient embolism in the lung capillaries, but dissociation will soon proceed and induce a loss of accumulated SiNPs and the dissociated particles subsequently redistribute to liver and spleen (Zhang et al. 2005). In our experiment the rapid reduction of SiNPs80 in lungs, and the redistribution of dissociated particles, probably contribute to the slow distribution changes of SiNPs80 in liver and spleen.

Despite the gradually decrease of SiNPs accumulation in liver and spleen, there was a significant amount of SiNPs remaining in these tissues at 30 days after injection. Why did the SiNPs remain in these tissues for over 30 days? We consider that the uptake by the cell in these tissues closely correlate with this question. Macrophages, part of the mononuclear phagocyte system (MPS), which locate primarily in the liver, spleen, lungs, and bone marrow, are involved in the uptake and metabolism of foreign molecules and particulates (Saba 1970). When

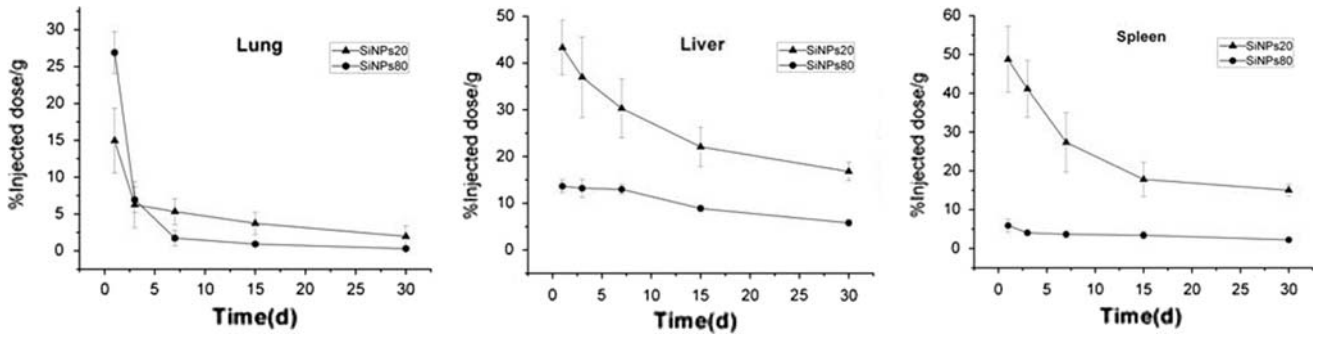

Fig. 4 The changes in distribution of SiNPs in lungs, liver and spleen

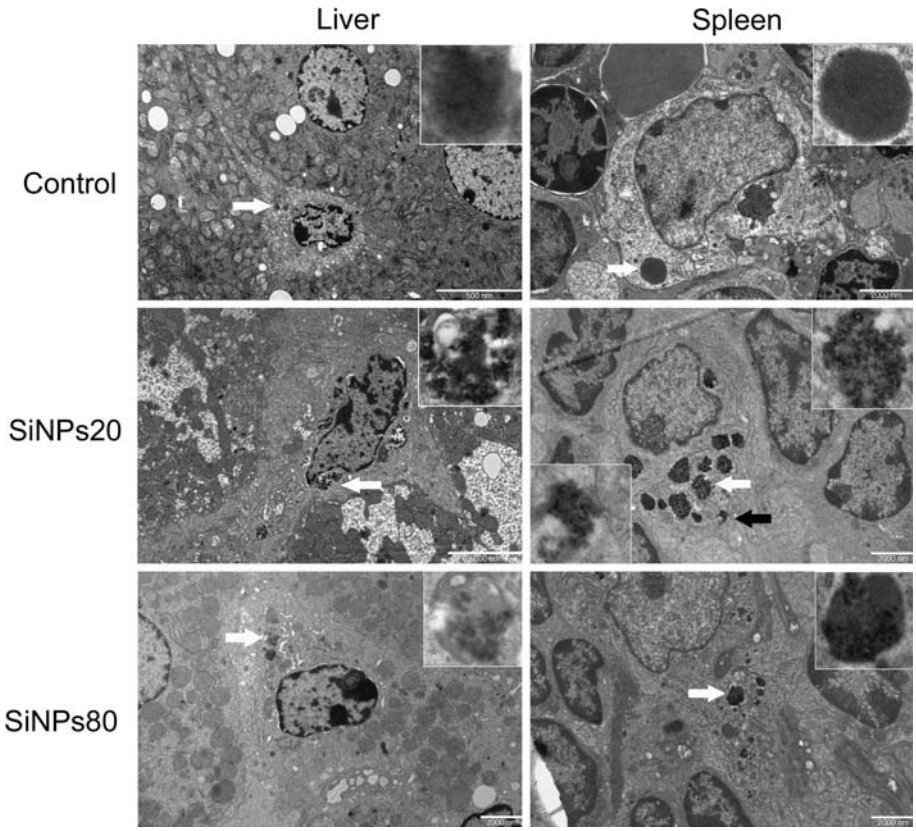

Fig. 5 TEM images of liver and spleen samples collected at 7 days after injection with two sizes of SiNPs. The *white arrows* denote phagolysosomes, and are magnified on the *upper right corner* of the same image. NPs were observed in the phagolysosomes of SiNP20 and SiNP80. The *black arrow* denote internalization, and are magnified on the *lower left corner* of the same image

nanoparticles are administered intravenously, a variety of serum proteins bind to the surface of the nanoparticles. They are recognized by the scavenger receptor on the macrophage cell surface and then internalized, leading to a significant loss of nanoparticles from the circulation (Opanasopit et al. 2002). The results of this study revealed that SiNPs were taken up mainly by macrophages in liver and spleen through endocytosis, and observed in phagosomes. The size of NPs has a role in cellular uptake (Chithrani et al. 2006; Nakai et al. 2003), the small size of NPs increase their uptake by cells (Chithrani and Chan 2007). This enhanced uptake of small NPs may largely attribute to the high surface potential of NPs, and increased presence at the cell membrane and binding to surface receptors. The high surface potential of small NPs increases protein binding and thus promote recognition by surface receptors. Small NPs also bind easily to surface receptors and wrapped by the membrane based on the competition between the thermodynamic driving force for wrapping and receptor diffusion kinetics (Bao and Bao 2005; Gao et al. 2005). These factors make small NPs easier to be taken up by macrophages and detained in the tissues than large NPs. Besides internalization, limited degradation of SiNPs in

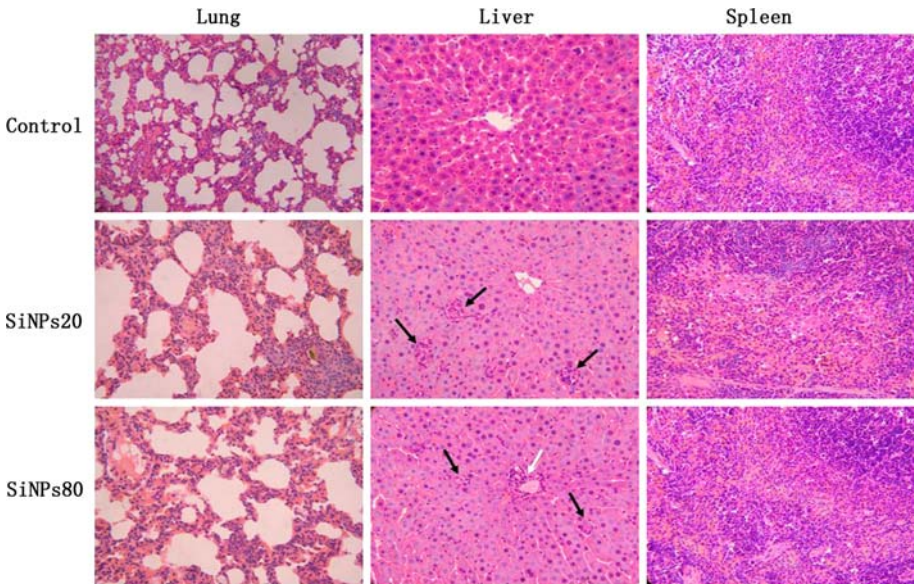

Fig. 6 Histological sections of lung, liver and spleen samples collected 1 week after sequential injections of SiNPs at 400× magnification. In the liver, a mononuclear inflammatory infiltrate (*white arrows*) at the portal area, and hepatocyte necrosis (*black arrows*) at the portal triads are observed

macrophages is an important role of SiNPs retention in tissues. Although macrophages can phagocytize and metabolize foreign molecules and particulates, the internalized SiNPs may resist this degradation because of their chemical stability. This limited degradation of SiNPs also contribute to the long-term retention in tissues.

We then considered whether SiNPs induce any damage to tissues when present at high doses long term. The results of toxicologic assay indicated that an inflammatory response and liver injury occurred after injection of SiNPs, suggesting potential side effects involving the liver. The inflammatory response may result from the internalization of SiNPs into macrophages and the subsequent activation of those macrophages (Aderem 2003). Although SiNPs are not taken up by hepatocytes in vivo, hepatocyte necrosis could be induced by the inflammatory response and the cytokines released from activated macrophages, such as TNF-α and IL-6.

Conclusions

In conclusion, we investigated the biodistribution, including long-term quantitative tissues distribution, subcellular distribution, and the toxicity of two sizes of intravenously administered SiNPs in vivo. The results of biodistribution indicated that SiNPs accumulated mainly in liver and spleen and retained in these tissues for over 30 days because of endocytosis by macrophages. Histological analysis showed that apparent pathological changes, including lymphocytic infiltration at the portal area and hepatocyte necrosis at the portal triads, were observed in the liver, suggesting potential side effects in the liver. Collectively, our investigation revealed that SiNPs accumulated and retained in MPS tissues due to macrophages in these tissues and were endocytosed by macrophages, and could produce side effects involving the liver injury. Based on the results of this study, further toxicologic investigations should be designed to evaluate the in vivo toxicity of SiNPs.

Acknowledgments This work was supported by grants from Natural Science Foundation of China (no. 30870680), Shanghai Sci-Tech Committee Foundation (no. 0752nm026) and Shanghai Leading Academic Discipline Project (no. S30206).

References

Aderem A (2003) Phagocytosis and the inflammatory response. J Infect Dis 187:S340–S345

Bagwe RP, Hilliard LR, Tan W (2006) Surface modification of silica nanoparticles to reduce aggregation and nonspecific binding. Langmuir 22:4357–4362

Bao G, Bao XR (2005) Shedding light on the dynamics of endocytosis and viral budding. Proc Natl Acad Sci USA 102:9997–9998

Chithrani BD, Chan WC (2007) Elucidating the mechanism of cellular uptake and removal of protein-coated gold nanoparticles of different sizes and shapes. Nano Lett 7:1542–1550

Chithrani BD, Ghazani AA, Chan WC (2006) Determining the size and shape dependence of gold nanoparticle uptake into mammalian cells. Nano Lett 6:662–668

Choi J, Burns AA, Williams RM, Zhou Z, Flesken-Nikitin A, Zipfel WR, Wiesner U, Nikitin AY (2007) Core-shell silica nanoparticles as fluorescent labels for nanomedicine. J Biomed Opt 12:064007

Fabian E, Landsiedel R, Ma-Hock L, Wiench K, Wohlleben W, van Ravenzwaay B (2008) Tissue distribution and toxicity of intravenously administered titanium dioxide nanoparticles in rats. Arch Toxicol 82:151–157

Fischer HC, Chan WC (2007) Nanotoxicity: the growing need for in vivo study. Curr Opin Biotechnol 18:565–571

Gao H, Shi W, Freund LB (2005) Mechanics of receptor-mediated endocytosis. Proc Natl Acad Sci USA 102:9469–9474

He X, Nie H, Wang K, Tan W, Wu X, Zhang P (2008) In Vivo Study of biodistribution and urinary excretion of surface-modified silica nanoparticles. Anal Chem 10:364–371

Hirsch LR, Stafford RJ, Bankson JA, Sershen SR, Rivera B, Price RE, Hazle JD, Halas NJ, West JL (2003) Nanoshell-mediated near-infrared thermal therapy of tumors under magnetic resonance guidance. Proc Natl Acad Sci USA 100:13549–13554

Huo Q, Liu J, Wang LQ, Jiang Y, Lambert TN, Fang E (2006) A new class of silica cross-linked micellar core-shell nanoparticles. J Am Chem Soc 128:6447–6453

Iezzi EB, Duchamp JC, Harich K, Glass TE, Lee HM, Olmstead MM, Balch AL, Dorn HC (2002) A symmetric derivative of the trimetallic nitride endohedral metallofullerene, Sc3N@C80. J Am Chem Soc 124:524–525

Jain TK, Reddy MK, Morales MA, Leslie-Pelecky DL, Labhasetwar V (2008) Biodistribution, clearance, and biocompatibility of iron oxide magnetic nanoparticles in rats. Mol Pharm 5:316–327

Kim J, Lee JE, Lee J, Yu JH, Kim BC, An K, Hwang Y, Shin CH, Park JG, Hyeon T (2006) Magnetic fluorescent delivery vehicle using uniform mesoporous silica spheres embedded with monodisperse magnetic and semiconductor nanocrystals. J Am Chem Soc 128:688–689

Li SD, Huang L (2008) Pharmacokinetics and biodistribution of nanoparticles. Mol Pharm 5:496–504

Li ZZ, Wen LX, Shao L, Chen JF (2004) Fabrication of porous hollow silica nanoparticles and their applications in drug release control. J Control Release 98:245–254

Lipski AM, Pino CJ, Haselton FR, Chen IW, Shastri VP (2008) The effect of silica nanoparticle-modified surfaces on cell morphology, cytoskeletal organization and function. Biomaterials 29:3836–3846

Mader H, Li X, Saleh S, Link M, Kele P, Wolfbeis OS (2008) Fluorescent silica nanoparticles. Ann NY Acad Sci 1130:218–223

Maynard AD, Aitken RJ, Butz T, Colvin V, Donaldson K, Oberdorster G, Philbert MA, Ryan J, Seaton A, Stone V, Tinkle SS, Tran L, Walker NJ, Warheit DB (2006) Safe handling of nanotechnology. Nature 444:267–269

Nakai T, Kanamori T, Sando S, Aoyama Y (2003) Remarkably size-regulated cell invasion by artificial viruses. Saccharide-dependent self-aggregation of glycoviruses and its consequences in glycoviral gene delivery. J Am Chem Soc 125:8465–8475

Oberdorster G, Oberdorster E, Oberdorster J (2005) Nanotoxicology: an emerging discipline evolving from studies of ultrafine particles. Environ Health Perspect 113:823–839

Opanasopit P, Nishikawa M, Hashida M (2002) Factors affecting drug and gene delivery: effects of interaction with blood components. Crit Rev Ther Drug Carrier Syst 19:191–233

Pham KN, Fullston D, Sagoe-Crentsil K (2007) Surface modification for stability of nano-sized silica colloids. J Colloid Interface Sci 315:123–127

Roy I, Ohulchanskyy TY, Bharali DJ, Pudavar HE, Mistretta RA, Kaur N, Prasad PN (2005) Optical tracking of organically modified silica nanoparticles as DNA carriers: a nonviral, nanomedicine approach for gene delivery. Proc Natl Acad Sci USA 102:279–284

Saba TM (1970) Physiology and physiopathology of the reticuloendothelial system. Arch Intern Med 126:1031–1052

Slowing II, Trewyn BG, Lin VS (2007) Mesoporous silica nanoparticles for intracellular delivery of membrane-impermeable proteins. J Am Chem Soc 129:8845–8849

Sonavane G, Tomoda K, Makino K (2008) Biodistribution of colloidal gold nanoparticles after intravenous administration: effect of particle size. Colloids Surf B Biointerfaces 66:274–280

Stern ST, McNeil SE (2008) Nanotechnology safety concerns revisited. Toxicol Sci 101:4–21

Torchilin VP, Lukyanov AN, Gao Z, Papahadjopoulos-Sternberg B (2003) Immunomicelles: targeted pharmaceutical carriers for poorly soluble drugs. Proc Natl Acad Sci USA 100:6039–6044

Tsuji JS, Maynard AD, Howard PC, James JT, Lam CW, Warheit DB, Santamaria AB (2006) Research strategies for safety evaluation of nanomaterials, part IV: risk assessment of nanoparticles. Toxicol Sci 89:42–50

Wang JJ, Sanderson BJ, Wang H (2007) Cyto- and genotoxicity of ultrafine TiO2 particles in cultured human lymphoblastoid cells. Mutat Res 628:99–106

Yang J, Lee J, Kang J, Lee K, Suh JS, Yoon HG, Huh YM, Haam S (2008) Hollow silica nanocontainers as drug delivery vehicles. Langmuir 24:3417–3421

Zhang JS, Liu F, Huang L (2005) Implications of pharmacokinetic behavior of lipoplex for its inflammatory toxicity. Adv Drug Deliv Rev 57:689–698

Zhao X, Hilliard LR, Mechery SJ, Wang Y, Bagwe RP, Jin S, Tan W (2004) A rapid bioassay for single bacterial cell quantitation using bioconjugated nanoparticles. Proc Natl Acad Sci USA 101:15027–15032